







Multinucleon transfer channels from ^{70}Zn (15 MeV/nucleon) + ^{64}Ni collisions

S. Koulouris,¹ G. A. Souliotis ^{1,*} F. Cappuzzello ^{2,3} D. Carbone,³ A. Pakou ⁴ C. Agodi ³ G. A. Brischetto,^{2,3} S. Calabrese,³ M. Cavallaro,³ I. Ciraldo,^{2,3} O. Fasoula,¹ J. Klimo,⁵ O. Sgouros ^{2,3} V. Soukeras ^{2,3} A. Spatafora,^{2,3} D. Torresi,³ and M. Veselsky⁶

¹Laboratory of Physical Chemistry, Department of Chemistry, National and Kapodistrian University of Athens, Athens, Greece

²Dipartimento di Fisica e Astronomia “Ettore Majorana”, Università di Catania, Catania, Italy

³Laboratori Nazionali del Sud, INFN, Catania, Italy

⁴Department of Physics and HINP, The University of Ioannina, Ioannina, Greece

⁵Institute of Physics, Slovak Academy of Sciences, Bratislava, Slovakia

⁶Institute of Experimental and Applied Physics, Czech Technical University, Prague, Czech Republic



(Received 13 June 2023; accepted 18 September 2023; published 18 October 2023)

In this article, we report a study of ejectile distributions of multinucleon transfer channels from the reaction of ^{70}Zn with ^{64}Ni at 15 MeV/nucleon. The measurements were performed with the MAGNEX large acceptance spectrometer in a wide angular range around the grazing angle and provided high-resolution characterization of the ejectiles in terms of the atomic number Z , the mass number A , the momentum-per-nucleon p/A , and the reaction angle θ_{lab} . The momentum distributions, angular distributions, and the production cross sections of several multinucleon transfer channels were extracted and studied in detail. Concerning the production of neutron-rich nuclides, that was one of the main motivations of this work, apart from proton-removal products, neutron-pickup isotopes (with up to three neutrons picked up from the target) were observed. The experimental distributions were compared with two dynamical models, the deep-inelastic transfer (DIT) model and the constrained molecular dynamics (CoMD) model, followed by the deexcitation code GEMINI. The DIT model, designed to describe the sequential exchange of nucleons, offered an overall fair description of the processes involving nucleon exchange, but was unable to describe the quasielastic part of the momentum distributions of several channels, suggesting the presence of direct reaction processes. The microscopic CoMD model gave an overall similar, but less accurate (with respect to DIT) description of the data, indicating that further development is needed. The present work outlines an experimental approach to investigate peripheral collisions of medium-mass heavy ions below the Fermi energy to extract information on the reaction mechanisms and provide guidance for the production of exotic neutron-rich nuclei.

DOI: [10.1103/PhysRevC.108.044612](https://doi.org/10.1103/PhysRevC.108.044612)

I. INTRODUCTION

Nuclei away from the valley of beta stability provide the opportunity to explore nuclear structure and nuclear dynamics at the extremes of neutron-to-proton asymmetry [1–6]. These extremes of the nuclear landscape—the drip lines—not only allow us to examine various aspects of the effective nuclear interaction, but also offer a venue to understand various astrophysical processes, most notably the rapid neutron capture process (r process). This explosive nucleosynthesis process, involving very neutron-rich nuclei from iron and above, takes place in stellar environments of high neutron flux and high temperature (e.g., supernova explosions, neutron star mergers) [7–9] and is responsible for approximately half of the abundance of nuclei heavier than iron.

For the last few decades, fragmentation, fission, and fusion reactions have been the traditional approaches to produce exotic nuclei in the laboratory [10–13]. In fact, the capabilities of these processes have effectively determined the present limits

of the nuclide chart [4]. Consequently, the efficient production of neutron-rich nuclides constitutes a central issue in current and future facilities worldwide (see, e.g., [14–22]).

To move further toward neutron-rich nuclides, along with proton stripping in the context of fragmentation, it is necessary to pick up neutrons from the target nucleus. This possibility is effectively offered by multinucleon transfer and deep-inelastic reactions between heavy ions at lower energies, namely near and above the Coulomb barrier. These reactions are characterized by the sequential exchange of nucleons between the projectile and the target and have been recently extensively used to access neutron-rich nuclei [23–26]. Concomitantly, multinucleon transfer reactions have been used to study the reaction mechanisms that lead to the production of these exotic nuclei (e.g., [27,28]). Thus, one can follow the evolution of the mechanism from quasielastic and direct processes to deep inelastic collisions characterized by high energy dissipation. We note that quasielastic processes include possible nucleon-pair transfer and thus, may elucidate the nucleon-nucleon correlations at energies around the Coulomb barrier [29,30].

*Corresponding author: soulioti@chem.uoa.gr

For effective exploration of multinucleon transfer reactions, especially those leading to rare nuclear species, modern magnetic spectrometers have been developed with large acceptance in momentum and solid angle. Examples of such devices are the following: PRISMA at INFN/LNL [31,32], VAMOS at GANIL [33–35], and MAGNEX at INFN/LNS [36–38].

Along the lines of the above studies, we investigated heavy-ion peripheral collisions at energies of 15–25 MeV/nucleon in order to access nuclides with high neutron excess. Initially, our studies involved 25 MeV/nucleon ^{86}Kr -induced reactions [39–42] and, subsequently, 15 MeV/nucleon ^{86}Kr -induced [43–45] and ^{40}Ar -induced reactions [46,47]. The aforementioned experiments were performed with the MARS recoil separator [48] at the Cyclotron Institute of Texas A&M University. Our studies indicated the limitations of a 0-degree separator to access the very neutron-rich fragments produced at angles around the grazing angle. Thus, for efficient collection and study of these fragments, the use of a large acceptance spectrometer is indispensable, as in the case of reactions near the Coulomb barrier.

In the energy range of 15–25 MeV/nucleon, the velocities of the ejectiles are higher and the angular distributions are narrower, compared to the Coulomb barrier reactions, leading to efficient collection and identification. Moreover, from a nuclear dynamics point of view, this energy regime differs from the regime near and above the Coulomb barrier, where a broad range of studies have already been performed and vividly continue. In the Fermi energy regime, the velocities of the reaction partners become comparable to the nucleon Fermi velocities, and the interaction time is shorter. This results in partial restriction of available phase space for nucleon transfer that takes place in this regime [49,50], compared to the Coulomb barrier reactions and implies the evolution of the reaction mechanism favoring faster and/or more dissipative dynamical processes.

Guided by these observations, we initiated a project to produce, identify, and measure the distributions of projectile-like fragments with the MAGNEX large-acceptance spectrometer at INFN-LNS from the reaction ^{70}Zn (15 MeV/nucleon) + ^{64}Ni . We note that the design of MAGNEX is optimized for charged particle spectroscopy, aiming at good energy and angular resolution and the ability to measure absolute cross sections for rare channels of interest [36,37]. In the present study, we relied on the performance of MAGNEX for reactions involving medium-mass heavy ions where the Z resolution appeared limited. As presented in Ref. [51], we developed a detailed procedure to reconstruct the atomic number Z of the ejectiles along with their ionic charge states employing measurements of the energy loss, residual energy, and time of flight. Subsequently, we proceeded to obtain the momentum and angular distributions of the ejectiles, and their production cross sections. These experimental results alongside comparisons to theoretical calculations will be presented in this article.

This work constitutes one of the very few high-resolution mass-spectrometric studies in the energy range of 15–25 MeV/nucleon, providing complete characterization of medium-mass ejectiles in terms of Z , A , velocity, and angle.

A similar mass-spectrometric study in this energy range, presented in [52–54], concerned ejectiles from the reaction of 18 MeV/nucleon ^{86}Kr with ^{208}Pb . We expect that the complete interpretation of the present data, along with detailed theoretical calculations and comparisons with previous work, will shed light on the evolution of the reaction mechanisms. Thus, our study will provide a bridge between the detailed studies of multinucleon transfer near and above the Coulomb barrier [23,24], and the large body of high-energy (fragmentation) reactions characterized by an abrasion-ablation mechanism [10].

The present article is organized as follows: In Sec. II, a description of the experimental setup and the measurements are presented. In Sec. III, the data analysis is described with emphasis on the identification of projectile-like fragments and extraction of their distributions. In Sec. IV, a description of the theoretical model framework is presented. Two dynamical models were used: the phenomenological deep-inelastic transfer (DIT) model and the microscopic constrained molecular dynamics model (CoMD). In Sec. V, the results on experimental distributions with emphasis on the neutron-rich nuclides are discussed along with comparisons to calculations. Finally, in Sec. VI, a discussion and conclusions are given.

II. EXPERIMENTAL DETAILS

The experiment was performed with the MAGNEX spectrometer [36,55,56] at Istituto Nazionale di Fisica Nucleare, Laboratori Nazionali del Sud (INFN-LNS) in Catania, Italy. A beam of $^{70}\text{Zn}^{15+}$ at 15 MeV/nucleon delivered by the K800 superconducting cyclotron bombarded a 1.18 mg/cm^2 ^{64}Ni foil at the optical object point of MAGNEX. The optical axis of the spectrometer was set at an angle of 9.0° , so MAGNEX covered the horizontal angular interval of 4.0° – 15.0° . We mention that its magnetic structure consists of a vertically focusing quadrupole and a horizontally dispersing and focusing dipole magnet. This apparatus provides a maximum acceptance in momentum of about 24% and in solid angle of 50 msr. The beam was collected in an electron suppressed Faraday cup inside the target chamber. The ejectiles emerging from the target passed through a $6\text{ }\mu\text{m}$ mylar stripper foil and then were momentum analyzed by the MAGNEX spectrometer [57–59] and detected by its focal plane detector (FPD) [60,61]. The FPD is a gas-filled hybrid detector providing the energy loss and the coordinates of the ions. At the end of the detector, a wall of 60 silicon detectors provides the residual energy of the ions. In our experiment, the Si detectors also provided the start for the time of flight (TOF) measurement of the ejectiles through the apparatus, while the stop signal was given by the radiofrequency (RF) of the cyclotron. This setup provided a TOF resolution of $\approx 3\text{ ns}$, limited mainly by the cyclotron RF timing.

In the present experiment, only about one-half of the active area of FPD was used in order to avoid radiation damage of the full array of the silicon detectors and possible high dead times due to limitations in the data acquisition system. Furthermore, to optimize the resolution, a set of vertical slits before the quadrupole restricted the vertical angular

acceptance of MAGNEX in the range -0.8° to 0.8° . This angular acceptance, along with the full horizontal angular acceptance (4° – 15°), implies a solid angle acceptance of 5.4 msr. The restriction of the vertical acceptance and the active area of the FPD resulted in the use of only seven of the silicon detectors belonging to the middle row of the silicon detector wall. We note that these experimental restrictions in the acceptance of the spectrometer will be circumvented in the future in view of the upgrade of MAGNEX [62]. Thus, in a full acceptance run, the whole area of the FPD can be exposed to the flux of the reaction products, allowing one to probe very suppressed reaction channels.

III. PARTICLE IDENTIFICATION AND ANALYSIS PROCEDURES

The projectile-like fragments from the studied reaction have atomic numbers $Z = 26$ – 32 and mass numbers $A = 60$ – 75 . The particle identification procedure is described in detail in [51,63,64]. Herein, we summarize the main points. The determination of the atomic number of the ejectiles involves a correlation between the total energy loss (ΔE_{cor}) in the gas section of the FPD (corrected for path length differences depending on the angle of incidence) and the residual energy measured by the silicon detectors (E_{resid}). In previous works with MAGNEX, this correlation was shown to be adequate for the determination of the atomic number Z of lighter ions (e.g., ^{18}O , ^{20}Ne , [65]). However, in our case of medium-mass heavy ions, this correlation was not adequate and we had to reconstruct the atomic number Z using the measured and calibrated quantities ΔE_{cor} , E_{resid} , and TOF, as presented in detail in [51]. The total kinetic energy is obtained as

$$E_{\text{tot}} = \Delta E_w + \Delta E_{\text{tot}} + E_{\text{resid}}, \quad (1)$$

where ΔE_{tot} is the measured energy loss and ΔE_w is a calculated correction for the energy loss in the entrance window of FPD. Furthermore, the TOF and the total energy information, along with the magnetic rigidity measurement allowed us to obtain the ionic charge state of the ion.

Subsequently, we employed a correlation of the reconstructed atomic number Z with the reconstructed ionic charge state q of the ejectiles in a two-dimensional plot and applied proper gating to select events of specific Z and q [51]. For the determination of the masses, we set gates on Z and q for each Si detector. We then implemented an approach of mass identification for large acceptance spectrometers as described in [36]. The approach relies on the relationship between the magnetic rigidity and the total kinetic energy of the ions, expressed as

$$B\rho = \frac{\sqrt{m}}{q} \sqrt{2E_{\text{tot}}}. \quad (2)$$

The proportionality of the magnetic rigidity $B\rho$ on $\sqrt{E_{\text{tot}}}$ with a slope of \sqrt{m}/q suggests that a correlation of $B\rho$ with $\sqrt{E_{\text{tot}}}$ or, equivalently, on E_{tot} , should lead to particle bands of the

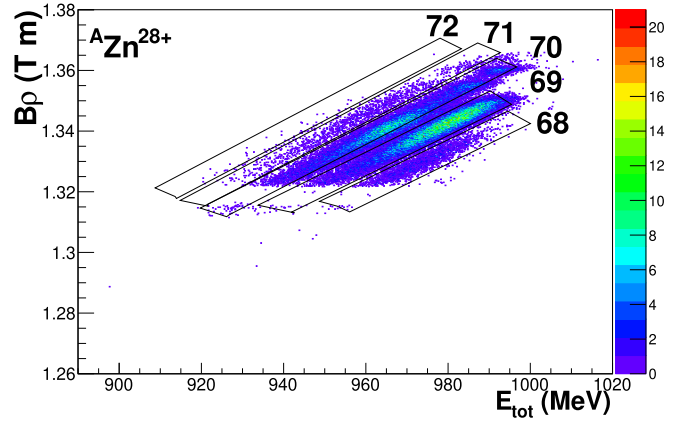


FIG. 1. Magnetic rigidity ($B\rho$) vs total energy (E_{tot}) correlation of ejectiles with $Z = 30$ and $Q = 28$ from the reaction ^{70}Zn (15 MeV/nucleon) + ^{64}Ni from one Si detector. The graphical contours represent isotopes of Zn^{28+} with $A = 68$ – 72 .

same \sqrt{m}/q . Since in our approach we have fixed q , the bands should refer to successive masses.

In Fig. 1, we present a typical plot of $B\rho$ versus E_{tot} for Zn^{28+} ejectiles (setting gates for $Z = 30$, $q = 28$) for events from one of the Si detectors. In this representation, the selection of the various masses is performed by setting the respective graphical cuts, as shown for $A = 68$ – 72 in the case of Zn^{28+} ejectiles.

After identification of all observed ejectiles on each Si detector, we proceeded with the analysis as follows. For each ion characterized by Z , q , and A , we obtained a two-dimensional distribution of the reaction angle θ_{lab} versus magnetic rigidity $B\rho$. These distributions were properly stored for subsequent analysis. Two representative examples are shown in Fig. 2 for $^{70}\text{Zn}^{28+}$ and $^{71}\text{Zn}^{28+}$ from the same Si detector as in Fig. 1.

We note that, in this experiment, we collected fragments at several magnetic rigidity settings covering the range from $B\rho_{\text{min}} = 1.260$ T m to $B\rho_{\text{max}} = 1.425$ T m. The beam current was continuously recorded and integrated. In a first step, the beam charge was used to obtain relative normalization between the various runs. To obtain absolute cross sections, regarding the horizontal angular acceptance, we employed the method of [58]. For that, we obtained and used elastic scattering data of 15 MeV/nucleon $^{70}\text{Zn} + ^{64}\text{Ni}$ and $^{70}\text{Zn} + ^{208}\text{Pb}$ at angles where the scattering is expected to be pure Rutherford scattering (specifically, for $^{70}\text{Zn} + ^{64}\text{Ni}$, this is valid only for $\theta_{\text{lab}} \leq 5^\circ$). We note that for the present experimental setup, the limited vertical angular acceptance of $\Delta\phi = 1.6^\circ$ did not imply any efficiency variation over the accepted phase space.

For a given nuclide Z, A at a given velocity bin—expressed in our analysis as momentum per nucleon p/A —and a given angular bin, θ_{lab} , the yields at its various charge states present in the data were combined in the following way. For each charge state q , a factor representing the fraction of the yield in this charge state, was obtained employing the parametrization of charge state distributions of Leon *et al.* [66]. This

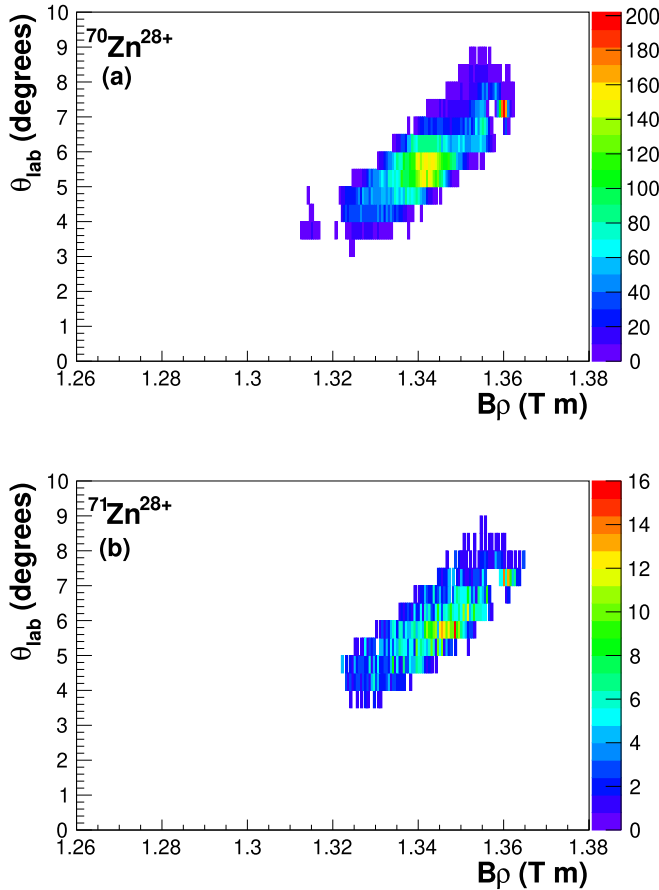


FIG. 2. Reaction angle θ_{lab} versus magnetic rigidity $B\rho$ of fully identified ejectiles from the reaction ^{70}Zn (15 MeV/nucleon) + ^{64}Ni , for the same Si detector as in Fig. 1. The ejectiles, with A gates shown in Fig. 1, correspond to $Z = 30$, $Q = 28$, and $A = 70$ (a), and $Z = 30$, $Q = 28$, and $A = 71$ (b).

parametrization of equilibrium charge state distributions has been successfully used in the energy and mass regime of our studies [39,40,43,67]. Employing these factors, the corrected yields represented by each charge state were obtained and averaged.

The above analysis procedure eventually resulted in a four-dimensional distribution of the differential cross section with respect to Z , A , θ_{lab} , and p/A . The bin widths of θ_{lab} and p/A were 0.5° and 0.5 MeV/ c , respectively. From this distribution, we obtained momentum and angular distributions as well as production cross sections of the ejectiles. We wish to comment that in our analysis and subsequent presentation we chose to use the momentum per nucleon (p/A) of the ejectiles, instead of the kinetic energy. The momentum per nucleon essentially expresses the velocity of the ejectiles and allows a direct comparison with the velocity of the beam. Moreover, similarly to the kinetic energy, it constitutes a good measure of the energy dissipation and can provide important information on the reaction mechanism. Experimental results on the distributions of various channels will be presented in the following, along with comparisons with theoretical models that will be, first, outlined in the next section.

IV. BRIEF DESCRIPTION OF THE THEORETICAL MODELS

The calculations performed in this work are based on a standard two-stage Monte Carlo approach. In the first, dynamical stage, the interaction between the projectile and the target was described by two theoretical models: the phenomenological DIT model and the microscopic CoMD model.

The DIT (deep-inelastic transfer) model [68] is a phenomenological model designed to describe peripheral collisions in the Fermi energy domain. Both the projectile and the target are assumed to be spherical and approach each other along Coulomb trajectories until they are within the range of the nuclear interaction. Then, the system is represented as two Fermi gases in contact allowing the stochastic exchange of nucleons through a “window” that opens between the touching nuclear surfaces. These nucleon transfers are responsible for the dissipation of the kinetic energy of relative motion into internal excitation and collective rotation of the primary fragments. The DIT code was run with its standard parameters [44,47] in the impact parameter range $b = 4\text{--}12$ fm. After separation, the two primary fragments, namely, the excited projectile-like and target-like fragments—that we also call, respectively, quasiprojectile (QP) and quasitarget—share approximately equally the total excitation energy.

The CoMD (constrained molecular dynamics) model [69,70] is a microscopic code for heavy-ion nuclear reactions from the Coulomb barrier to the Fermi energy and above. The code is based on the general approach of quantum molecular dynamics (QMD) [71] describing the nucleons as localized Gaussian wave packets that interact via an effective nucleon-nucleon interaction. In this model, the enforcement of the Pauli principle is achieved via a phase space constraint at each step of the time evolution of the system. The CoMD code was run with parameters as in our recent work [47], employing an effective interaction with a compressibility of $K = 254$ MeV. The impact parameter range was $4\text{--}12$ fm and the time evolution of the system was followed for times up to 600 fm/ c (2×10^{-21} s).

After the dynamical stage of the reaction, described by either of the above two models, the deexcitation of the primary fragments was described by the GEMINI code. GEMINI is a statistical deexcitation code that implements Monte Carlo techniques and the Hauser-Feshbach formalism to calculate the probabilities for fragment emission with $Z \leq 2$ [72,73] (see also [44]). Heavier fragments may be emitted with probabilities following a transition state formalism. The final partition of products is generated by a succession of binary decays.

In the following, the two-stage DIT/GEMINI and CoMD/GEMINI calculations will be referred to as DIT and CoMD calculations, respectively.

V. EXPERIMENTAL RESULTS AND COMPARISON WITH MODEL CALCULATIONS

In this section, we present the experimental results of ejectile distributions from the reaction of ^{70}Zn with ^{64}Ni at 15 MeV/nucleon obtained from the analysis described in Sec. III.

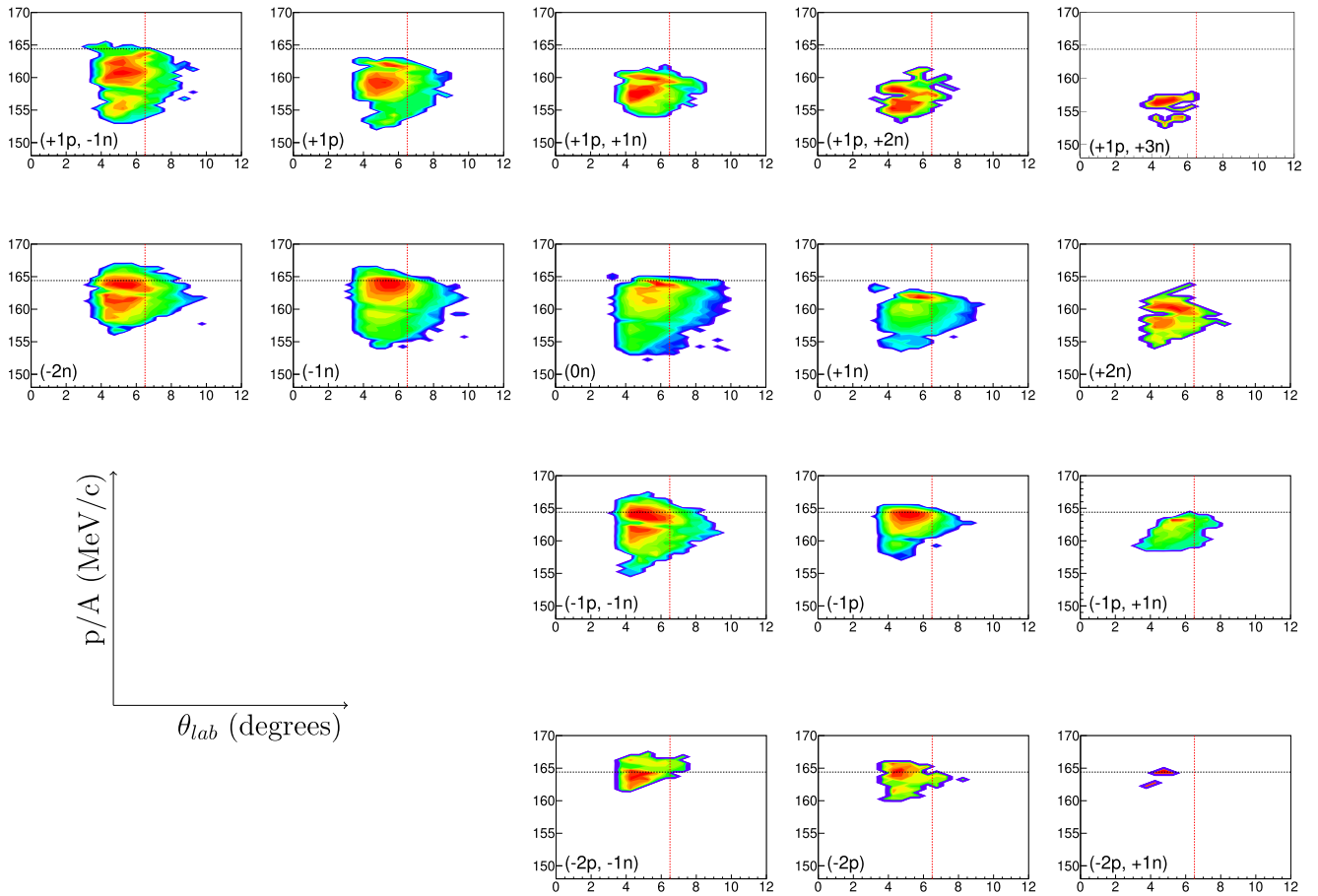


FIG. 3. Wilczynski plots of ejectiles from representative channels of the reaction ^{70}Zn (15 MeV/nucleon) + ^{64}Ni . The horizontal lines represent the p/A of the projectile and the vertical lines the grazing angle. Channels are marked by the number of neutrons or protons added or removed from the projectile. The inelastic channel, denoted as “0n” (corresponding to no net nucleon transfer) is also displayed.

Further on, we proceed with a comparison of the experimental data with theoretical calculations employing the models presented in Sec. VI.

Recall that the analysis of the data resulted in ejectile distributions (differential cross sections) with respect to Z , A , θ_{lab} , and p/A . In order to have an overall perspective of the distributions for most of the isotopes analyzed, we present two-dimensional distributions of p/A versus θ_{lab} in Fig. 3. These plots—that we will refer to as Wilczynski plots in our discussion—are essentially equivalent to the traditional Wilczynski plots. The latter are plots of kinetic energy versus scattering angle widely used in the study of deep-inelastic collisions near and above the Coulomb barrier providing information on energy dissipation and the dynamical behavior of the dinuclear complex [74–76]. In the plots of Fig. 3, the horizontal lines represent the projectile $p/A = 164.4$ MeV/c, and the vertical lines indicate the grazing angle $\theta_{\text{gr}} \simeq 6.5^\circ$ of the ejectiles of the reaction [77]. The various channels are marked by the number of neutrons or protons added or removed from the projectile. For our orientation, the channel of ^{70}Zn , corresponding to no net nucleon transfer, that we will call “inelastic” channel, is displayed in the middle panel. In most of the channels we discern a peak (a “band”) near

the velocity of the beam (quasielastic peak) and an extended region of lower velocities corresponding to more dissipative events, as we will discuss in further detail later. In addition, in most of the channels we observe characteristic valleys along the θ_{lab} coordinate, or correspondingly dips in the distributions along the p/A coordinate (as we will also see later). These dips are the result of the software gates imposed during the data analysis to remove the elastically scattered beam, as we have already mentioned. As we may expect, the nucleon pickup products are characterized by overall lower p/A values (velocities) essentially due to momentum conservation, as these projectile-like fragments have picked up nucleons from the “stationary” target. We note here that a velocity shift for nucleon pickup products has been also observed at higher (fragmentation) energies (80–140 MeV/nucleon) [78,79] and interpreted with a simple momentum conservation model. We also note that the distributions peak at and near the grazing angle. This fact reveals the quasielastic and deep-inelastic character of the production mechanism.

At this point, we will not discuss these plots further. Instead, we will consider, first, the integration of these distributions with respect to p/A that will give angular distributions (to be discussed later), whose further integration

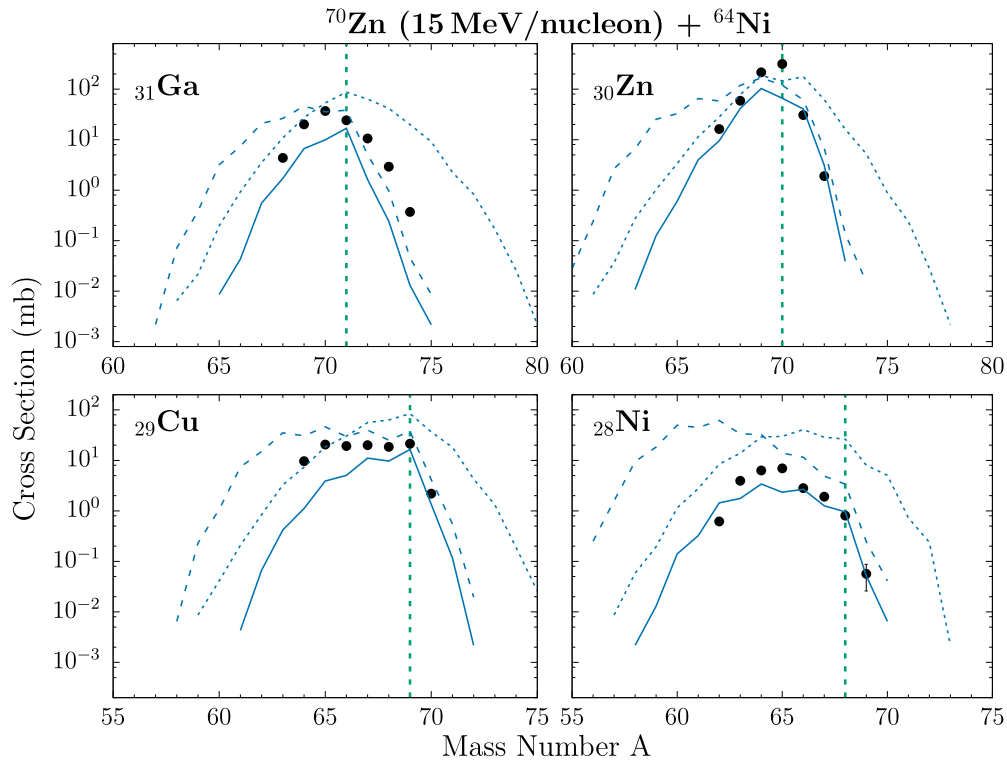


FIG. 4. Mass distributions (cross sections) of elements with $Z = 28\text{--}31$ from the reaction ^{70}Zn (15 MeV/nucleon) + ^{64}Ni . The experimental data are shown by closed (black) circles. The DIT calculations are shown as follows: primary fragments with dotted (blue) line, final (cold) fragments with dashed (blue) line, and final fragments filtered for acceptance with the solid (blue) line (see text). The vertical dashed (green) line indicates the initiation of neutron pickup.

with respect to θ_{lab} will provide the production cross sections of the observed nuclides. Moreover, we will proceed with integration of these two-dimensional distributions over θ_{lab} in an appropriate window that will result in the p/A distributions.

A. Production cross sections

In Figs. 4 and 5, we present the production cross sections for the observed isotopes of the elements with $Z = 28\text{--}31$ from the reaction ^{70}Zn (15 MeV/nucleon) with ^{64}Ni . In both figures, the experimental data are shown by the full black points. The vertical dashed (green) line indicates the beginning of neutron pickup that develops from this line to the right.

As we see from these figures (and also from Fig. 3), in the present experiment, we achieved the production and complete characterization—in terms of Z , A , p/A , and θ_{lab} —of several neutron-rich nuclides corresponding to the pickup of 2–3 neutrons from the target.

The distinct advantage of employing the MAGNEX spectrometer is the high-resolution measurement of the reaction angle and the momentum resulting from the trajectory reconstruction procedure. This detailed angular and momentum information is decisive for the elucidation of the reaction mechanisms, as we have already noticed in regards to Fig. 3, and we will elaborate in the following.

We now compare the experimental cross sections with the DIT and CoMD calculations presented in Figs. 4 and 5, respectively. Recall that the calculations are performed in a Monte Carlo fashion leading to calculated distributions (differential cross sections) in terms of Z , A , p/A , and θ_{lab} . Moreover, ionic charge states can be assigned to the above distributions by employing the parametrization of charge state distributions of Leon *et al.* [66] that was also employed in the analysis of the experimental data (Sec. III). Thus, the calculated distributions can be appropriately projected (and/or integrated) so that they can be compared with the experimental data.

In Fig. 4, we first focus our attention to the calculated yield distributions of the primary projectile-like fragments (quasiprojectiles) presented by the dotted (blue) lines. We observe wide and nearly symmetric distributions extending far to the neutron-rich side. The deexcitation of these excited primary products with the GEMINI code leads to the (cold) nuclides with cross sections depicted by the dashed (blue) lines. The distributions of these final nuclides are substantially altered compared to those of the primary nuclides (especially on their neutron-rich side) and are closer to the experimental data. As a general observation, the symmetric shape of the primary yield distributions bears some similarity to that of the yield distributions of products from multinucleon transfer reactions near the Coulomb barrier [23,24,27]. However, at our energy, the excitation energies of the primary products are

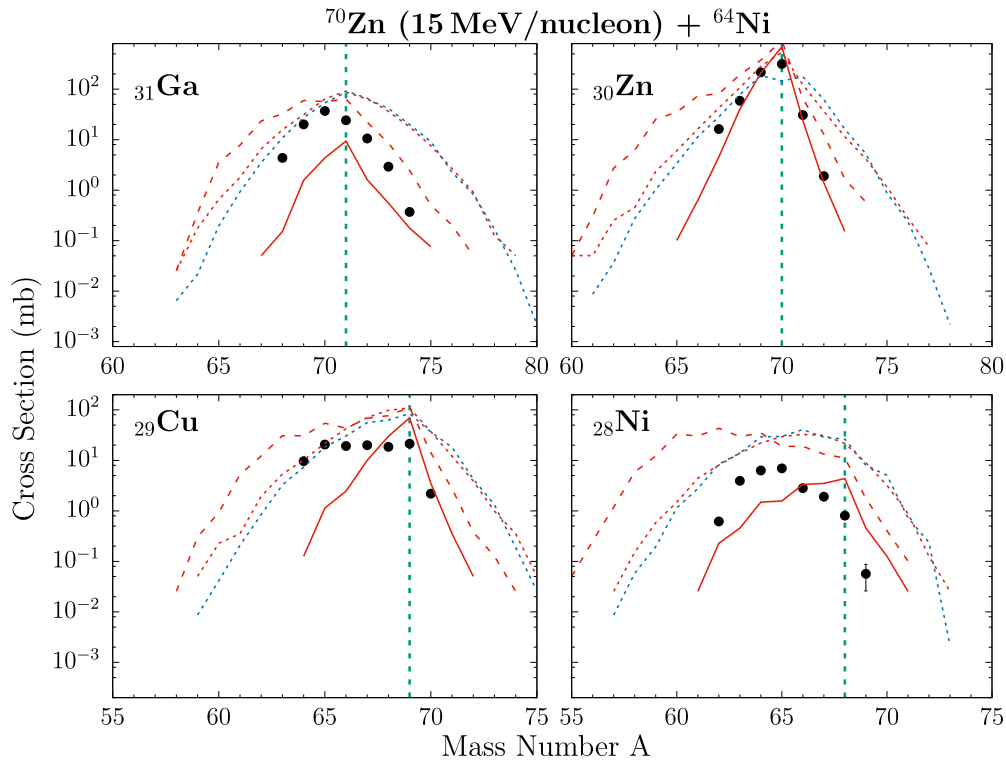


FIG. 5. Mass distributions (cross sections) of elements with $Z = 28 - 31$ from the reaction ^{70}Zn (15 MeV/nucleon) + ^{64}Ni . The experimental data are shown by closed (black) circles. Here, the CoMD calculations are shown as follows: primary fragments with dotted (red) line, final (cold) fragments with dashed (red) line, and final fragments filtered for acceptance with the solid (red) line (see text). For comparison, primary fragments from DIT are repeated with the dotted (blue) line. The vertical dashed (green) line indicates the initiation of neutron pickup.

expected to be higher and the evaporation chains longer, thus leading to substantially altered final yield distributions.

Furthermore, in Fig. 4, with solid (blue) lines we show the cross sections after filtering the theoretical distributions for the angular acceptance of MAGNEX ($\Delta\theta_{\text{lab}} = 4^\circ - 15^\circ$) and the magnetic rigidity interval 1.260–1.425 T m covered in the experiment, as mentioned before.

Interestingly, we observe that the filtered DIT calculations lead to cross sections that are in overall reasonable agreement with the experimental data. The neutron-rich sides of the distributions are rather well described, with the exception of the Ga ($Z = 31$) isotopes (one-proton pickup). On the neutron-deficient side, we see that both the filtered distributions and the data are much lower than the calculated total (i.e., without filtering) cold yield distributions (dashed lines in the figure). This is obviously an effect of the limited $B\rho$ range covered in the present experiment. Our calculations show that the minimum $B\rho$ should be 1.000 T m in order to cover the full range of the neutron deficient nuclides.

In Fig. 5, we present the CoMD calculations and their comparison to the data in a fashion similar to the DIT ones. The dotted (red) lines show the CoMD primary yields directly compared to the DIT primary yields (dotted blue lines) that are also repeated in this figure. It is interesting to notice that the two primary fragment distributions are nearly identical, especially on the neutron-rich side. This result suggests that

the overall effect of nucleon transfer (exchange) and the mass flow are effectively similar in both models, despite the different physical ingredients of them. As in Fig. 4, here again the dashed (red) lines show the cross sections after the GEMINI deexcitation stage, and the full (red) lines show the filtered cross sections.

Our remark concerning the CoMD calculations is that while they provide, to some extent, an overall description of the shape of the experimental yield distributions, they tend to overpredict the yields of the neutron-rich sides of the distributions for the isotopes below the projectile.

Given the observed similarity in the calculated primary yields between DIT and CoMD, we tentatively ascribe the observed differences in the cross sections to possible differences in the excitation energies of the primary products.

Despite the overall better agreement of DIT with the experimental cross section data, we will continue to present and evaluate the results from both codes in the following discussion. It is our intention to further understand and improve the CoMD results by possible proper choice of the parameters of the model and investigation of the excitation energy distributions of the primary products.

We notice that the present results do not extend as far out toward neutron-rich nuclides as our previous measurements with the 15 MeV/nucleon ^{86}Kr beam on ^{64}Ni and ^{124}Sn with the MARS separator [43,44], due to severe limitations in the

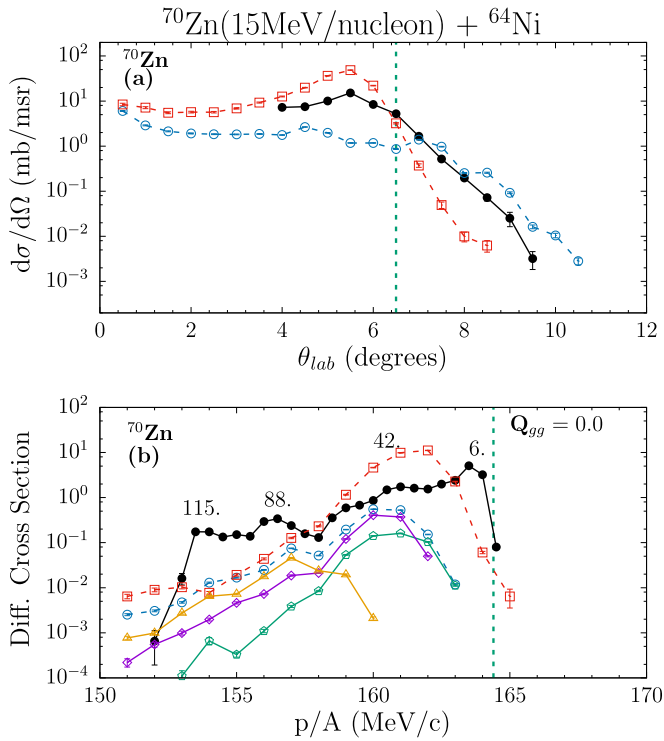


FIG. 6. (a) Angular distribution of ejectiles from the inelastic channel of the reaction ^{70}Zn (15 MeV/nucleon) + ^{64}Ni . The experimental data are shown by closed (black) circles. The vertical dashed (green) line indicates the grazing angle. The calculations shown are DIT by open (blue) circles and CoMD by open (red) squares. (b) Momentum per nucleon distribution of ejectiles from the inelastic channel. The experimental data are shown by closed (black) circles. The vertical dashed (green) line is the p/A of the projectile. The numbers above some peaks give the total excitation energy (in MeV) obtained from binary kinematics using the corresponding p/A values. The DIT calculation is shown with open (blue) circles and the CoMD one by open (red) squares. Three components of the DIT distribution, that we call QP-0n, QP-1n and QP-2n, are shown under the assumption that the primary fragment (the quasiprojectile, QP) undergoes pick up of no neutrons [open (green) squares], one neutron [open (purple) diamonds] and, two neutrons [open (yellow) triangles] and subsequent evaporation of them (see also text).

beam current imposed by the experimental setup in which the elastically scattered projectiles were accepted in the focal plane detector. This limitation will be circumvented in the future in view of the ongoing upgrade of MAGNEX [62] toward accepting high rates that will be crucial in order to extend our experimental studies to very neutron-rich nuclides.

B. Inelastic channel

In Fig. 6, we present the angular and momentum distributions of ^{70}Zn ejectiles. We will refer to this channel as the “inelastic” channel, including possible complicated processes of nucleon pickup, breakup, and evaporation which end up with no net nucleon transfer from the target to the projectile. We will come back to this point later on. In Fig. 6(a), we present the angular distribution of the inelastic channel. The experimental data are shown by the closed points. The

vertical dashed line indicates the grazing angle $\theta_{\text{gr}} = 6.5^\circ$. As already mentioned, the elastically scattered projectiles have been removed by software gates, and thus do not contribute. This angular distribution has the characteristic shape of a quasielastic process peaking just inside the grazing angle, as is the case for the angular distributions of most of the observed channels. We also compare the experimental distribution with the results from the DIT and CoMD calculations shown by open (blue) circles and open (red) squares, respectively. The DIT calculations exhibit a rather flat behavior underestimating the data, while extending to larger angles. The CoMD calculations tend to overestimate the data, while they describe the peak of the data inside the grazing angle.

We continue with a discussion of the momentum per nucleon, p/A , distributions starting from the inelastic channel ^{70}Zn , displayed in Fig. 6(b). The experimental data are shown by the closed points. The vertical dashed line indicates the p/A of the projectile. We note that the horizontal axis gives the p/A in steps of 0.5 MeV/c, representing a momentum resolution of $\approx 0.3\%$. To obtain the p/A distributions, we integrated the experimental distributions in the angular range $\theta_{\text{lab}} = 4^\circ - 6^\circ$, corresponding to the region around the peak of the distributions. The vertical axis, denoted as “diff. cross section,” gives the value of $\frac{d^2\sigma}{d(p/A)d\Omega}$ in units of $\frac{\text{mb}}{(\text{MeV}/c)\text{msr}}$. We have verified that if we obtain the p/A distributions of this channel in the full observation window of $\theta_{\text{lab}} = 4^\circ - 15^\circ$, the shape of the spectrum remains almost unchanged and the differential cross section is only slightly higher. This is valid for all reaction channels involved in this work.

The numbers above some of the peaks give the total excitation energy of the quasiprojectile-quasitarget system obtained using the indicated p/A values and employing binary kinematics. The excitation energy is connected to the reaction Q value as $E_{\text{tot}}^* = Q_{\text{gg}} - Q$, where Q_{gg} is the ground-state to ground-state Q value of the channel, reported on the right side of the p/A figure.

The quasielastic peak corresponding to $E_{\text{tot}}^* = 6$ MeV represents inelastic excitation of the projectile and/or the target to low-lying states with a combined excitation energy of this value. The bump at $E_{\text{tot}}^* = 42$ MeV corresponds to more complicated processes possibly involving the pickup of a neutron from the projectile and the subsequent evaporation of a neutron to yield the ^{70}Zn nucleus. In a similar fashion, as in the detailed analysis of Sohlbach *et al.* [52] we can assume that the bump at $E_{\text{tot}}^* = 88$ MeV corresponds to the pickup of two neutrons from the projectile and a subsequent evaporation. We will come back to this point later on by decomposing our DIT calculations into various processes.

In the same figure, along with the experimental data, we show the DIT calculation with open (blue) circles. We note that the theoretical DIT distributions were filtered taking into account the $B\rho$ range of the experiment and the polar (horizontal) angular window $\theta_{\text{lab}} = 4^\circ - 6^\circ$ that we chose for the integration of the experimental p/A distributions, as already mentioned. Furthermore, since the experimental azimuthal angle window was $\Delta\phi_{\text{lab}} = 1.6^\circ$, and no filter for the above azimuthal acceptance was applied in the calculations, we downscaled the theoretical distribution by an appropriate az-

imuthal factor (≈ 20) before comparing it to the experimental p/A distribution. [This factor is the ratio of the solid angles subtended in the corresponding two cases of polar angular window $\theta_{\text{lab}} = 4^\circ\text{--}6^\circ$ and azimuthal angular windows of 360° , and $\Delta\phi_{\text{lab}} = 1.6^\circ$.]

We observe that the DIT calculation can describe only the part of the distribution from the first bump at $p/A = 161$ MeV/ c ($E_{\text{tot}}^* = 42$ MeV) and lower. This result is consistent with the fact that DIT has no inherent mechanism of inelastic excitation, thus it cannot describe the inelastic part of the experimental p/A spectrum. Recall that the only process that is treated by the DIT model is the sequential transfer of nucleons from the projectile to the target and vice versa.

To elaborate further on the DIT calculation, we present in Fig. 6(b) the decomposition of the p/A distributions of the ejectiles predicted by DIT under the assumption that they come from primary quasiprojectiles that have picked up no neutrons (green squares), one neutron (purple diamonds), and two neutrons (yellow triangles), respectively, and lost an equal number of neutrons in subsequent evaporation. We will refer to these calculations as QP- λn , where $\lambda = 0, 1, 2$, denoting that the observed ejectile comes from a primary fragment (quasiprojectile, QP) which (after appropriate pickup) has evaporated no neutrons, one neutron, and two neutrons, respectively. The first two of these distributions peak near the experimental bump of $E_{\text{tot}}^* = 42$ MeV, with the QP- $0n$ channel contributing 29% and the QP- $1n$ channel contributing 52% of the total DIT distribution. The QP- $2n$ channel (with 13% contribution) peaks at lower p/A values in correspondence with the observed bump at $E_{\text{tot}}^* = 88$ MeV, albeit the higher yield of the latter. The dip in the data at $p/A = 158$ MeV/ c due to the exclusion of elastically scattered projectiles can also be described by the DIT calculation, provided that we impose a software gate to exclude elastically scattered projectiles with $q = 29$ in the calculation.

We notice that between the left side of the inelastic peak of $E_{\text{tot}}^* = 6$ MeV and the right side of the peak of the DIT distribution corresponding to $E_{\text{tot}}^* = 42$ MeV, there is an area of the spectrum that is not accounted for by either of the above two contributions. We tentatively assign this part of the distribution to higher-energy inelastic excitation of the target nucleus to the giant resonance regime possibly involving double (or higher order) resonances (see, e.g., [80] and references therein). A similar contribution may be assumed for the part of the experimental spectrum corresponding to the bump of $E_{\text{tot}}^* = 88$ MeV and to lower p/A values, including the edge of $E_{\text{tot}}^* = 115$ MeV which is near the lower limit of the magnetic rigidity of the experiment. Further analysis to extract the relevant contributions is not a straightforward task and is beyond the scope of the present article.

Furthermore, in Fig. 6(b), we show the CoMD calculation (open squares). The CoMD calculation is higher and broader than DIT, extending to larger p/A values toward the experimental quasielastic peak. Despite the overall disparity of the CoMD calculation with respect to the data and the DIT calculation, we wish to point out that, owing to its fully microscopic N -body character, the model has the inherent ability to describe inelastic excitation (in a gross manner;

CoMD predicts no discrete states), as well as giant resonances [81] and the collective response of the projectile and the target induced by their mutual interaction. This dynamical behavior of CoMD requires further investigation [82]. Along these lines, from an experimental point of view, investigation of a collective dipole mode, the so-called dynamical dipole mode, was recently performed (e.g., [83,84] and references therein) via measurements of preequilibrium γ ray emission of the projectile and target after their interaction. In close relation to these studies, we foresee that the coupling of the MAGNEX spectrometer with the proposed G-NUMEN array [85–87] will enable further studies of preequilibrium aspects in combination with fully identified ejectiles.

C. Nucleon removal and nucleon pickup channels

We will now continue with the presentation of the p/A distributions of some of the most important transfer channels observed, and later on with the corresponding angular distributions. In Fig. 7, we show the p/A distributions of several nucleon removal products. Specifically, we present the products obtained from the removal of one neutron (^{69}Zn), one proton (^{69}Cu), two neutrons (^{68}Zn), and two protons (^{68}Ni). As we discussed before, the observed dips in the p/A spectra are due to software gates in our analysis to exclude elastically scattered beam particles.

Concerning the one-neutron removal ($-1n$) and the one-proton removal ($-1p$) channels, the experimental p/A distributions have rather similar shapes (apart from the abrupt ending of the second in its left side, due to experimental $B\rho$ restrictions). However, we observe a large difference in the cross sections of the $-1n$ and $-1p$ channels, the former being one order of magnitude higher than the latter. In these distributions, we observe a distinct quasielastic peak just below the projectile velocity corresponding to low E_{tot}^* and a lower bump corresponding to higher E_{tot}^* , in analogy to the situation regarding the inelastic channel [Fig. 6(b)].

Focusing our attention to the $-1n$ channel, we assign the first peak at $p/A = 164$ MeV/ c and $E_{\text{tot}}^* = 11$ MeV to a direct process of one neutron stripping from the ^{70}Zn projectile. Furthermore, we may assign the part of the distribution below $p/A = 162$ MeV/ c to a multistep process involving the pickup of one neutron, leading to an excited primary ejectile of ^{71}Zn , and the subsequent evaporation of two neutrons. This analysis is corroborated by the DIT calculation presented in the same manner as in Fig. 6(b) for the inelastic channel. We notice that the DIT calculation is lower than the data, but the shape the quasielastic peak is reasonably well described by the QP- $0n$ component of the calculation. The QP- $1n$ and QP- $2n$ components reasonably well describe the lower part of the distribution and the bump at $E_{\text{tot}}^* = 69$ MeV, but they are again lower than the data. The contributions of the above three components relative to the total DIT distribution are 63%, 17%, and 11%, respectively.

Analogous remarks pertain to the $-1p$ channel. The quasielastic peak represents a direct proton stripping, and the part at lower velocities comes from a more complex process involving, apart from proton removal, neutron pickup and

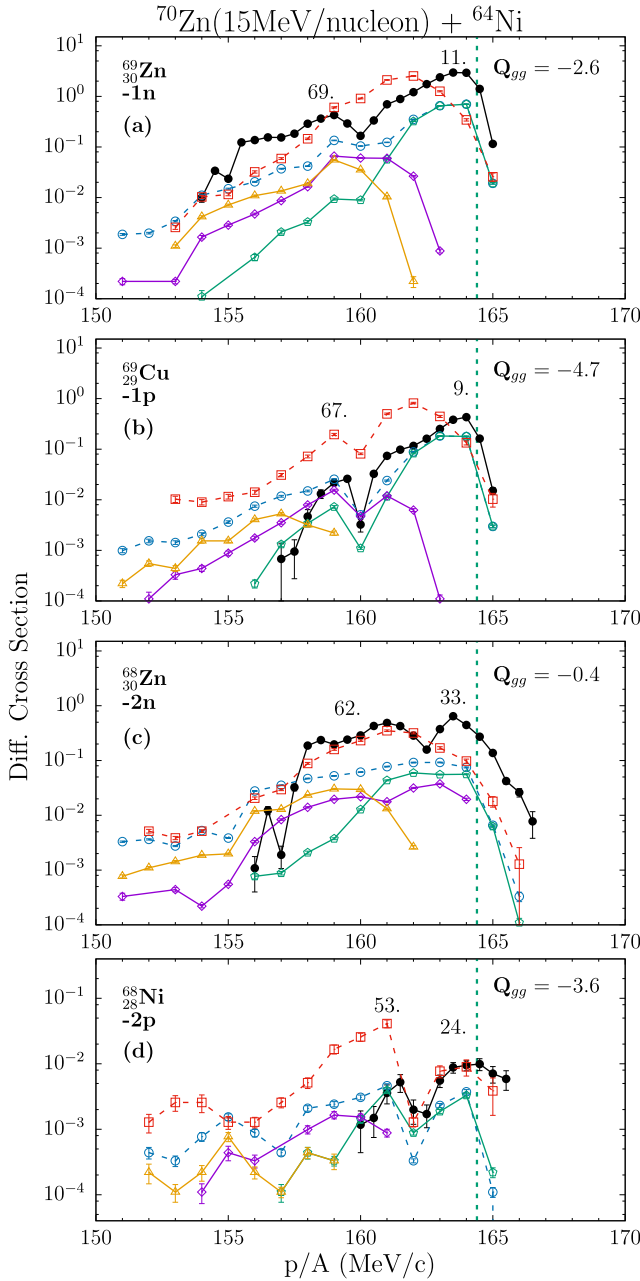


FIG. 7. Momentum per nucleon distributions of ejectiles from stripping channels of the reaction ^{70}Zn (15 MeV/nucleon) + ^{64}Ni . The experimental data are shown by closed (black) circles. The vertical dashed (green) line is the p/A of the projectile. The DIT calculation is shown by open (blue) circles, and the CoMD one by open (red) squares. The three components of the DIT distribution, namely QP-0n, QP-1n, and QP-2n, are also shown with open (green) squares, open (purple) diamonds and, open (yellow) triangles, respectively, as in Fig. 6(b).

subsequent evaporation, corroborated by the DIT analysis, as above.

It is interesting to note that the DIT calculation adequately describes the experimental p/A distributions of $-1n$ and $-1p$ channels, most notably the quasielastic part. This points to the overall fair description of the one nucleon stripping, that is the simplest process that can be described by the DIT model.

However, the discrepancy in the magnitude of the QE part of the $-1n$ channel may be ascribed to details of the direct processes that require proper analysis with direct reaction codes. Moreover, the discrepancy regarding the lower part of the $-1n$ spectrum may reflect collective excitations of the target, as in the case of the inelastic channel.

In regards to the CoMD model, the calculation results in peaks at velocities lower than those of the experimental quasielastic peaks, and appears to overestimate the distributions, especially the one-proton removal channel.

We now turn our attention to the two-neutron and two-proton removal channels, Figs. 7(c) and 7(d). The two spectra are rather similar, apart from the abrupt left side of the $-2p$ spectrum, the first one being about two orders of magnitude higher. For the $-2n$ channel, the DIT calculation underestimates both the quasielastic peak and the lower part of the p/A distribution. The QP- λn decomposition appears to yield approximately equal contributions ($\approx 23\%$) of the three components. Concerning the $-2p$ channel, the DIT calculation gives a somewhat better description of the experimental spectrum, but it also underestimates the QE side of the spectrum. The three QP- λn DIT components have contributions of 53%, 23%, and 12%, following the same trend as obtained for the $-1n$ and $-1p$ channels.

As in the case of reactions at lower energies (e.g., [30] and references therein), we may assume that a process of direct transfer of a nucleon pair (neutron pair or proton pair) contributes to the quasielastic part of these channels. The CoMD calculation appears to describe the $-2n$ spectrum, apart from its QE part. In contrast, it describes the QE part of the $-2p$ spectrum, but it overestimates the lower part, as in the case of the $-1p$ spectrum. A common observation regarding the left part of the $-1n$ and $-2n$ spectra is that the DIT calculation is substantially lower than the data. As already pointed out, this discrepancy may reflect contributions of collective excitations of the target residual that may be partially accounted for in the CoMD calculation.

In Figs. 8(a)–8(c), we present the p/A distributions of ejectiles with pickup of one proton, one neutron, and two neutrons from the target, whereas in Fig. 8(d) we show the p/A distribution for the single charge exchange channel. As in the case of nucleon removal channels, the spectra of the pickup products are characterized by a quasielastic peak, now located at velocities just below the beam—because of the nucleon pickup—and an extended part at lower velocities. The total excitation energies of the quasielastic peaks, as indicated in the figures, are low. The full calculations with DIT [open (blue) circles with dashed lines] appear to describe part of the quasielastic peak and the shape of the tails of these pickup channels.

Specifically, for the $+1p$ channel, the QP-0n component of the DIT distribution appears to describe only part of the quasielastic peak. In contrast, the QP-1n is not able to describe the broad experimental peak of $E_{\text{tot}}^* = 48$ MeV, indicating the inability of DIT to describe the proton pickup and/or the possible contribution of collective excitation of the target remnant in a way similar to the $-1n$, $-2n$, and the inelastic channels, discussed before.

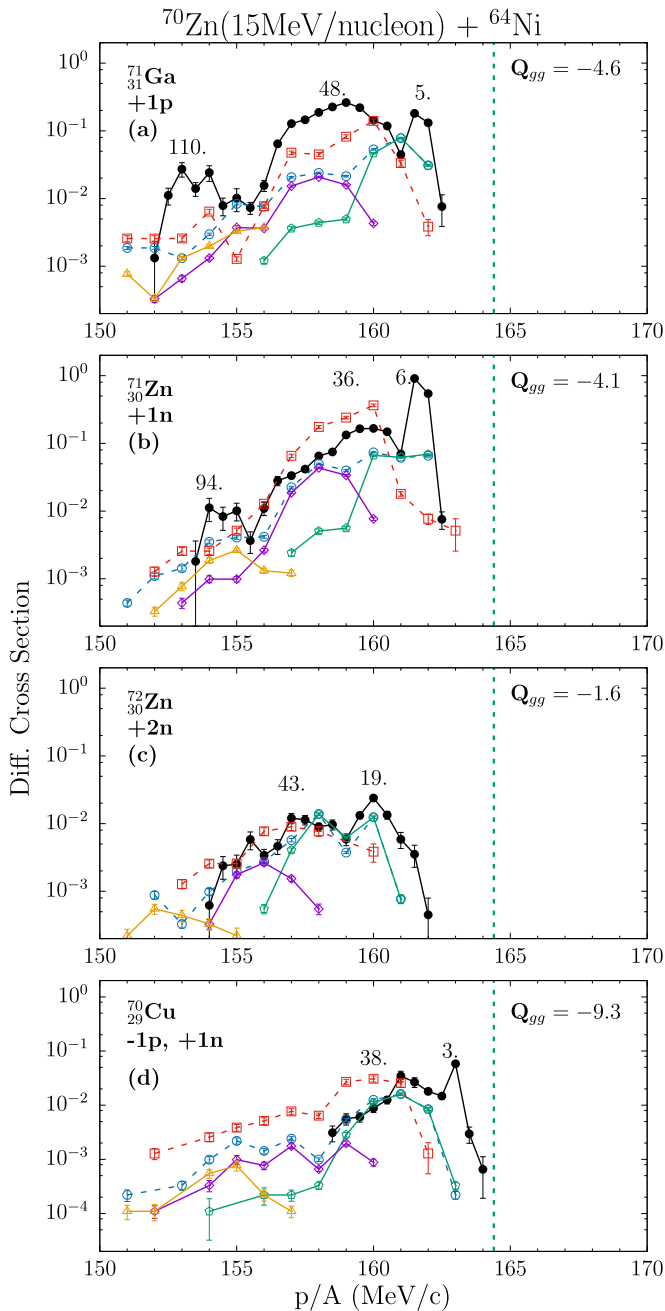


FIG. 8. Momentum per nucleon distributions of ejectiles from nucleon pickup channels of the reaction ^{70}Zn (15 MeV/nucleon) + ^{64}Ni . The experimental data are shown by closed (black) circles. The vertical dashed (green) line is the p/A of the projectile. The DIT calculation is shown by open (blue) circles, and the CoMD one by open (red) squares. The three components of the DIT distribution, namely QP-0n, QP-1n, and QP-2n, are also shown with open (green) squares, open (purple) diamonds and, open (yellow) triangles, respectively, as in Fig. 5.

Concerning the +2n channel, the QP-0n DIT calculation describes most of the quasielastic part of the spectrum, apart from its right side. The QP-1n component describes the lower part of the p/A spectrum. Again, this observation may suggest

the possibility of a direct neutron-pair pickup in the experimental data.

In Fig. 8(d), we present the p/A distribution of the isotope $^{70}\text{Cu}(-1p, +1n)$ involving single charge exchange. A sharp quasielastic peak appears just below the velocity of the projectile corresponding to very low excitation energy. It is noteworthy that the DIT calculation (the QP-0n component) appears to describe most of the experimental distribution, apart from the quasielastic peak. This may be taken as an indicator of a direct charge exchange process involving meson exchange (see, e.g., [88] and references therein) in addition to the nucleon exchange, the latter process being rather adequately described by DIT.

Regarding the CoMD calculation for all the channels of Fig. 8 [open (red) squares with dashed lines], the general behavior is that the calculated p/A distributions exhibit broad peaks at lower velocities than the data and appear to miss the QE part of the spectra.

For completeness in Figs. 9 and 10 we present the angular distributions of the nucleon removal and the nucleon pickup products, respectively. The data are given by the closed points, while the open points are the calculations. The vertical dashed (green) line represents the ejectile grazing angle $\theta_{\text{gr}} = 6.5^\circ$. As in the case for the inelastic channel [Fig. 6(a)], the angular distributions exhibit a bell-shaped pattern peaking inside the grazing angle. The DIT and CoMD calculations appear to describe the general behavior of the angular distributions. However, the DIT calculations are broader than the data, whereas the CoMD calculations are somewhat narrower and, specifically for the $-1p$ and $-2p$ channels, are higher than the data (as we also saw for the corresponding p/A distributions).

D. “Cluster” pickup products

In Fig. 11, we display the p/A distributions of isotopes of Ga ($Z = 31$). These correspond to the pickup of one proton and to one, two, and three neutrons from the target. We observe a progressive displacement of the quasielastic peak to lower velocities with increasing number of nucleons picked up, due to momentum conservation. Both the DIT and the CoMD calculations cannot describe the experimental distributions for these channels, grossly underestimating the data. This may suggest that, apart from the sequential pickup of nucleons, the contribution of direct pickup of clusters (d , ^3H , etc.) from the target should be taken into account. Such a process is not described by the DIT or the CoMD models and motivates further theoretical investigation with appropriate models explicitly involving cluster degrees of freedom [89–91].

VI. DISCUSSION AND CONCLUSIONS

In this article we present our study of the reaction $^{70}\text{Zn} + ^{64}\text{Ni}$ at 15 MeV/nucleon with the MAGNEX spectrometer. This is our first effort to study peripheral collisions with medium-mass heavy ions with a large acceptance spectrometer in this energy. The ejectiles were fully characterized in terms of the atomic number Z , the mass number A , the momentum per nucleon p/A and the reaction

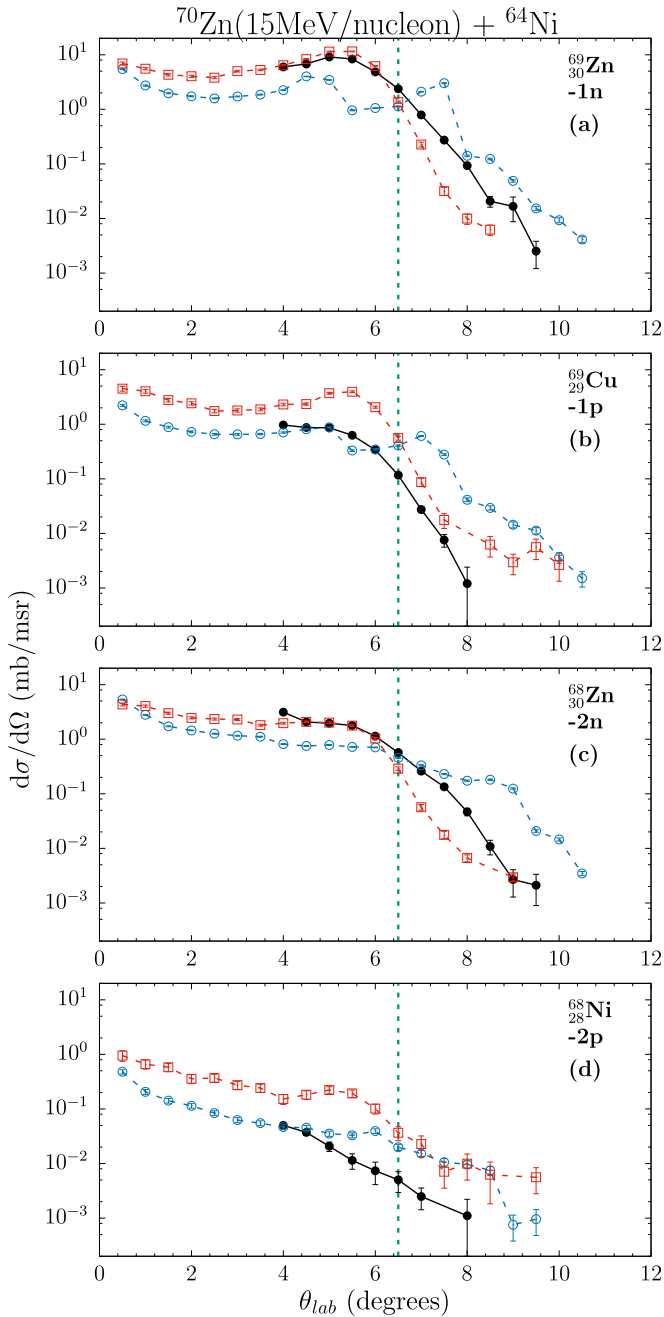


FIG. 9. Angular distributions of ejectiles from stripping channels of the reaction ^{70}Zn (15 MeV/nucleon) + ^{64}Ni . The experimental data are shown by closed (black) circles. The vertical dashed (green) line shows the grazing angle. The calculations shown are DIT by open (blue) circles and CoMD by open (red) squares.

angle θ_{lab} . The momentum distributions, angular distributions, and the production cross sections of several multinucleon transfer channels were extracted and studied in detail. The high-resolution momentum and angular information of the present data was decisive for elucidation of the reaction mechanisms.

The overall picture of the reaction mechanism outlined in a first glance with the Wilczynski plots indicates mainly two processes: (a) a quasielastic process characterized by

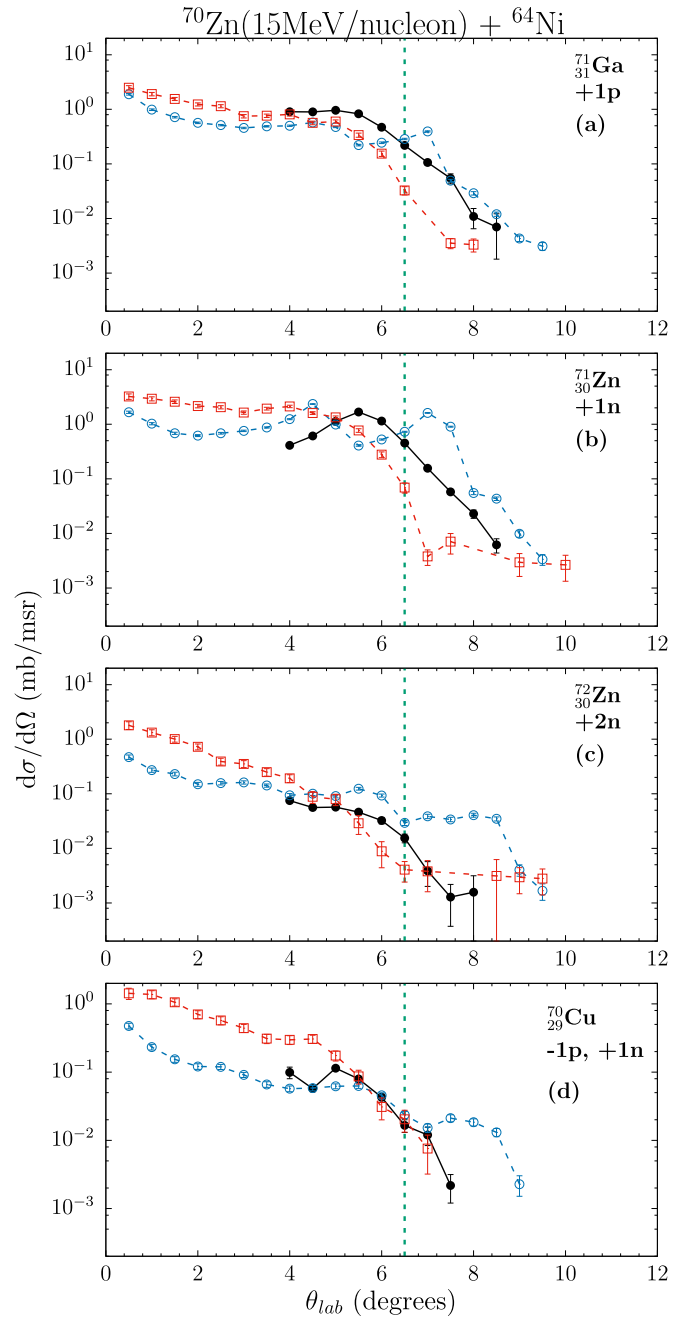


FIG. 10. Angular distributions of ejectiles from nucleon pickup channels of the reaction ^{70}Zn (15 MeV/nucleon) + ^{64}Ni . The experimental data are shown by closed (black) circles. The vertical dashed (green) line shows the grazing angle. The calculations shown are DIT by open (blue) circles and CoMD by open (red) squares.

velocities just below the projectile velocity and low excitation energy (nucleon stripping seems to be in favor of this process) and (b) an extended region of lower velocities and high excitation energies (nucleon pickup seems to be in favor of this process). We should underline here, that the deep-inelastic region, involves dissipative processes, i.e., more complicated processes of nucleon exchange and subsequent neutron evaporation. Since both processes, quasielastic and deep inelastic,

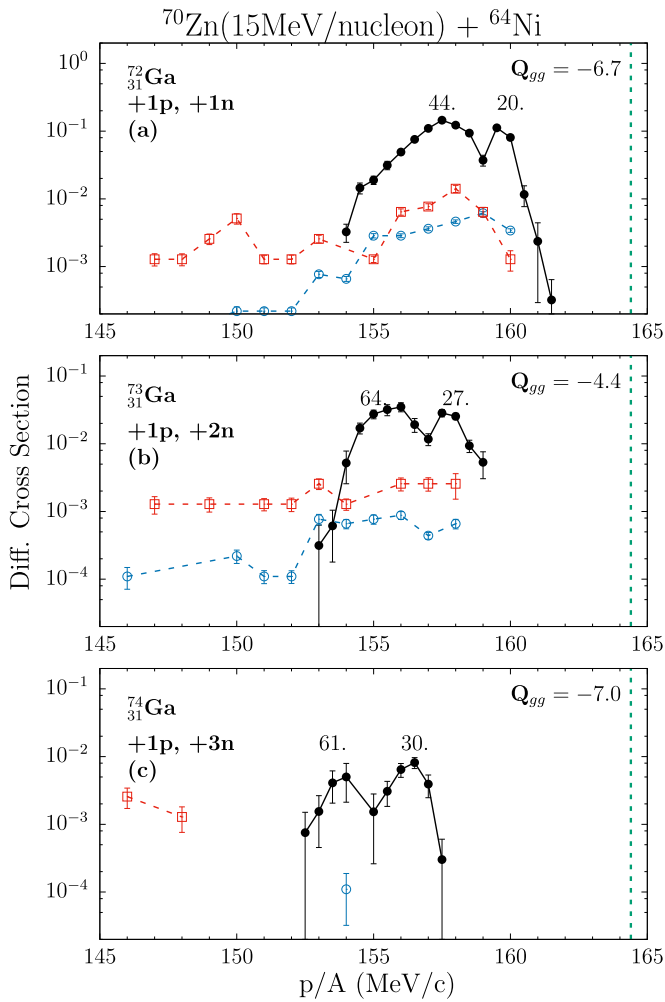


FIG. 11. Momentum per nucleon distributions of ejectiles from “cluster” pickup channels of the reaction ^{70}Zn (15 MeV/nucleon) + ^{64}Ni . The experimental data are shown by closed (black) circles. The vertical dashed (green) line is the p/A of the projectile. The calculations shown are DIT by open (blue) circles and CoMD by open (red) squares.

were observed in all our reaction products, a deconvolution of those was attempted successfully and various channel contributions were determined.

In this first experiment with MAGNEX, we achieved the production of several neutron-rich nuclides close to the projectile. We note that during the experiment the elastically scattered projectiles, after traversing the spectrometer, were accepted by the focal plane detector. This experimental condition imposed limitation in the beam current in regards to the production of more neutron-rich nuclides. However, in the present work, the MAGNEX facility offered the distinct advantage of the high-resolution measurement of the momentum and the reaction angle of the medium mass ejectiles in an extended region covering the quasielastic and deep-inelastic processes. We wish to mention that the ongoing upgrade of the MAGNEX focal plane detector toward high rates will be advantageous to extend our experimental studies to more neutron-rich nuclides in the near future. Along this line, the

coupling of the upgraded MAGNEX spectrometer with the proposed G-NUMEN array [85–87] will allow, among other aspects, the study of γ rays in coincidence with fully identified ejectiles in the MAGNEX spectrometer, allowing detailed exploration of the reaction dynamics, as well as the spectroscopy of the produced nuclides.

The experimental data of this work were compared with two dynamical models, the DIT and the CoMD, followed by the deexcitation code GEMINI. The DIT model, designed to describe the sequential exchange of nucleons, offered an overall fair description of the processes involving nucleon exchange, but could not describe the quasielastic part in some of the channels, most notably the inelastic channel, the two-nucleon removal channels and the single-nucleon exchange channel. Furthermore, it grossly underestimated channels that may correspond to the pickup of clusters. The CoMD model gave an overall, but less accurate description of the data, indicating that further developments are needed.

Our future plans include the use of direct reaction codes such as FRESKO [92] and/or PTOLEMY [93] for further understanding of the reaction processes involved in this system and energy regime. Also, we plan to test the semiclassical code GRAZING [94,95], widely used to describe reactions near and above the Coulomb barrier.

The present work represents our first step that paves the way to detailed studies of peripheral reactions of medium-mass nuclei in the Fermi energy regime. This regime is characterized by velocities of the reaction partners comparable to the nucleon Fermi velocities and, thus, shorter interaction times, compared to the Coulomb barrier reactions. The reaction mechanism evolves toward favoring faster and/or more dissipated dynamical processes. As examples of fast processes, that were hinted by our experimental data in comparison with our models, we report (a) the high-energy inelastic excitation in the region of giant resonances, possibly involving multiphonon excitations, (b) the direct transfer of nucleon (neutron or proton) pairs, (c) the meson-mediated single charge exchange and, (d) the direct transfer of clusters between the reaction partners. Each of these interesting processes is a nuclear dynamics topic by itself and shows the exciting possibilities for subsequent near-term investigations inspired by the present work along with future experimental and theoretical studies.

In closing, we envision that the ensuing studies in this energy and mass regime will probe the evolution of the various facets of nuclear dynamics, and play an overarching role between the investigations of multinucleon transfer near the Coulomb barrier and the studies of high-energy (fragmentation) reactions. Furthermore, these studies will provide guidance to the efficient production of exotic neutron-rich nuclei toward the r -process path and the neutron drip line.

ACKNOWLEDGMENTS

We are grateful to the support staff of INFN–LNS for providing the primary beam. This project has received funding from the European Research Council (ERC) under the European Union’s Horizon 2020 research and innovation program (Grant Agreement No 714625). G.S. and S.K. acknowledge

support from the Special Account for Research Grants of the National and Kapodistrian University of Athens. M.V. was

supported by the Czech Science Foundation (GACR) Grant No. 21-24281S.

-
- [1] S. R. Stroberg, J. D. Holt, A. Schwenk, and J. Simonis, *Ab initio* limits of atomic nuclei, *Phys. Rev. Lett.* **126**, 022501 (2021).
- [2] Q. Z. Chai, Y. Qiang, and J. C. Pei, Correlations between nuclear landscape boundaries and neutron-rich *r*-process abundances, *Phys. Rev. C* **105**, 034315 (2022).
- [3] T. Mijatovic, Multinucleon transfer reactions: a mini-review of recent advances, *Front. Phys.* **10**, 965198 (2022).
- [4] G. G. Adamian, N. V. Antonenko, A. Diaz-Torees, and S. Heinz, How to extend the chart of nuclides?, *Eur. Phys. J. A* **56**, 47 (2020).
- [5] Y. X. Watanabe, Y. H. Kim, S. C. Jeong, Y. Hirayama, N. Imai, H. Ishiyama *et al.*, Pathway for the production of neutron-rich isotopes around the $N = 126$ closure, *Phys. Rev. Lett.* **115**, 172503 (2015).
- [6] F. Nowacki, A. Obertelli, and A. Poves, The neutron-rich edge of the nuclear landscape: Experiment and theory, *Prog. Part. Nucl. Phys.* **120**, 103866 (2021).
- [7] A. Arcones and F. K. Thielemann, Origin of the elements, *Astron. Astrophys. Rev.* **31**, 1 (2023).
- [8] J. J. Cowan, C. Sneden, J. E. Lawler, A. Aprahamian, M. Wiescher, K. Langanke, G. Martinez-Pinedo, and F. K. Thielemann, Origin of the heaviest elements: The rapid neutron-capture process, *Rev. Mod. Phys.* **93**, 015002 (2021).
- [9] H. Grawe, K. Langanke, and G. Martinez-Pinedo, Nuclear structure and astrophysics, *Rep. Prog. Phys.* **70**, 1525 (2007).
- [10] C.-W. Ma, H.-L. Wei, X.-Q. Liu, J. Su, H. Zheng, W.-P. Lin *et al.*, Nuclear fragments in projectile fragmentation reactions, *Prog. Part. Nucl. Phys.* **121**, 103911 (2021).
- [11] S. Heinz and H. M. Devaraja, Nucleosynthesis in multinucleon transfer reactions, *Eur. Phys. J. A* **58**, 114 (2022).
- [12] Y. Blumenfeld, T. Nilsson, and P. V. Duppen, Facilities and methods for radioactive ion beam production, *Phys. Scr. T* **152**, 014203 (2013).
- [13] J. Erler, N. Birge, M. Kortelainen, W. Nazarewicz, E. Olsen, A. M. Perhac *et al.*, The limits of nuclear landscape, *Nature (London)* **486**, 509 (2012).
- [14] FRIB main page, www.frib.msu.edu.
- [15] GANIL main page, www.ganil.fr.
- [16] GSI main page, www.gsi.de.
- [17] RIBF, www.nishina.riken.jp/facility/RIBFabout_e.html.
- [18] ATLAS, www.phy.anl.gov/atlas/facility/index.html.
- [19] INFN/LNS main page, www.lns.infn.it.
- [20] RISP main page, www.risp.re.kr/eng/pMainPage.do.
- [21] K. Tshoo, H. Chae, J. Park, J. Y. Moon, Y. K. Kwon, G. A. Souliotis *et al.*, Design status of KOBRA for rare isotope production and direct measurements of radiative capture cross sections, *Nucl. Instrum. Methods B* **376**, 188 (2016).
- [22] N. S. Martorana, G. Cardella, C. Guazzoni, E. V. Pagano, A. D. Russo, P. Rusotto *et al.*, Radioactive ion beam opportunities at the new FRAISE facility of INFN-LNS, *Front. Phys.* **10**, 1058419 (2022).
- [23] L. Corradi, G. Pollarolo, and S. Szilner, Multinucleon transfer processes in heavy-ion reactions, *J. Phys. G: Nucl. Part. Phys.* **36**, 113101 (2009).
- [24] L. Corradi, S. Szilner, G. Pollarolo, D. Montanari, E. Fioretto, A. M. Stefanini *et al.*, Multinucleon transfer reactions: Present status and perspectives, *Nucl. Instrum. Methods B* **317**, 743 (2013).
- [25] J. Diklic, S. Szilner, L. Corradi, T. Mijatovic, G. Pollarolo, P. Colovic *et al.*, Transfer reactions in $^{206}\text{Pb} + ^{118}\text{Sn}$: From quasielastic to deep-inelastic processes, *Phys. Rev. C* **107**, 014619 (2023).
- [26] R. M. Perez-Vidal, F. Galtarossa, T. Mijatovic, S. Szilner, I. Zanon, D. Brugnara *et al.*, Nuclear structure advancements with multinucleon transfer reactions, *Eur. Phys. J. A* **59**, 114 (2023).
- [27] T. Mijatovic, S. Szilner, L. Corradi, D. Montanari, G. Pollarolo, E. Fioretto *et al.*, Multinucleon transfer reactions in the $^{40}\text{Ar} + ^{208}\text{Pb}$ system, *Phys. Rev. C* **94**, 064616 (2016).
- [28] F. Galtarossa, L. Corradi, S. Szilner, E. Fioretto, G. Pollarolo, T. Mijatovic *et al.*, Mass correlation between light and heavy reaction products in multinucleon transfer $^{197}\text{Au} + ^{130}\text{Te}$ collisions, *Phys. Rev. C* **97**, 054606 (2018).
- [29] D. Montanari, L. Corradi, S. Szilner, G. Pollarolo, E. Fioretto, G. Montagnoli *et al.*, Neutron pair transfer in $^{60}\text{Ni} + ^{116}\text{Sn}$ far below the Coulomb barrier, *Phys. Rev. Lett.* **113**, 052501 (2014).
- [30] L. Corradi, S. Szilner, G. Pollarolo, T. Mijatovic, D. Montanari, E. Fioretto *et al.*, Evidence of proton-proton correlations in the $^{116}\text{Sn} + ^{60}\text{Ni}$ transfer reactions, *Phys. Lett. B* **834**, 137477 (2022).
- [31] D. Montanari, E. Farnea, S. Leoni, G. Pollarolo, L. Corradi, G. Benzoni *et al.*, Response function of the magnetic spectrometer PRISMA, *Eur. Phys. J. A* **47**, 4 (2011).
- [32] T. Mijatovic, S. Szilner, L. Corradi, D. Montanari, G. Pollarolo, E. Fioretto *et al.*, Study of the cross section determination with the PRISMA spectrometer: The $^{40}\text{Ar} + ^{208}\text{Pb}$ case, *Eur. Phys. J. A* **52**, 113 (2016).
- [33] H. Savajols, VAMOS: a VArIable MOde high acceptance Spectrometer for identifying reaction products induced by SPIRAL beams, *Nucl. Instrum. Methods B* **204**, 146 (2003).
- [34] S. Pullanhiotan, M. Rejmund, A. Navin, W. Mittig, and S. Bhattacharyya, Performance of VAMOS for reactions near the Coulomb barrier, *Nucl. Instrum. Methods A* **593**, 343 (2008).
- [35] M. Rejmund, B. Lecornu, A. Navin, C. Schmitt, S. Damoy, O. Delaune *et al.*, Performance of the improved larger acceptance spectrometer: VAMOS ++, *Nucl. Instrum. Methods A* **646**, 184 (2011).
- [36] F. Cappuzzello, C. Agodi, D. Carbone, M. Cavallaro, The MAGNEX spectrometer: Results and perspectives, *Eur. Phys. J. A* **52**, 167 (2016).
- [37] F. Cappuzzello, C. Agodi, M. Cavallaro, D. Carbone, S. Tudisco, D. Lo Presti *et al.*, The NUMEN project: NUClear Matrix Elements for Neutrinoless double beta decay, *Eur. Phys. J. A* **54**, 72 (2018).
- [38] F. Cappuzzello, H. Lenske, M. Cavallaro, C. Agodi, N. Auerbach, J. I. Bellone *et al.*, Shedding light on nuclear aspects of neutrinoless double beta decay by heavy-ion double charge exchange reactions, *Prog. Part. Nucl. Phys.* **128**, 103999 (2023).
- [39] G. A. Souliotis, M. Veselsky, G. Chubarian, L. Trache, A. Keksis, E. Martin, A. Ruangma, E. Winchester, and S. J. Yennello, Enhanced production of neutron rich rare isotopes in

- the reaction of 25 MeV/nucleon ^{86}Kr on ^{64}Ni , *Phys. Lett. B* **543**, 163 (2002).
- [40] G. A. Souliotis, M. Veselsky, G. Chubarian, L. Trache, A. Keksis, E. Martin, D. V. Shetty, and S. J. Yennello, Enhanced production of neutron-rich rare isotopes in peripheral collisions at Fermi energies, *Phys. Rev. Lett.* **91**, 022701 (2003).
- [41] G. A. Souliotis, M. Veselsky, G. Chubarian, and S. J. Yennello, Production and separation of neutron-rich rare isotopes around and below the Fermi energy, *Nucl. Instrum. Methods B* **204**, 166 (2003).
- [42] G. A. Souliotis, A. L. Keksis, B. C. Stein, M. Veselsky, M. Jandel, D. V. Shetty, S. N. Soisson, S. Wuenschel, and S. J. Yennello, Neutron-rich rare isotope production in the Fermi energy domain and application to the Texas A&M radioactive beam upgrade, *Nucl. Instrum. Methods B* **266**, 4692 (2008).
- [43] G. A. Souliotis, M. Veselsky, S. Galanopoulos, M. Jandel, Z. Kohley, L. W. May, D. V. Shetty, B. C. Stein, and S. J. Yennello, Approaching neutron-rich nuclei toward the r -process path in peripheral heavy-ion collisions at 15 MeV/nucleon, *Phys. Rev. C* **84**, 064607 (2011).
- [44] P. N. Fountas, G. A. Souliotis, M. Veselsky, and A. Bonasera, Systematic study of neutron-rich rare isotope production in peripheral heavy-ion collisions below the Fermi energy, *Phys. Rev. C* **90**, 064613 (2014).
- [45] O. Fasoula, G. A. Souliotis, S. Koulouris, K. Palli, M. Veselsky, S. Yennello, and A. Bonasera, Study of multinucleon transfer mechanisms in ^{86}Kr -induced peripheral reactions at 15 and 25 MeV/nucleon, *HNPS Adv. Nucl. Phys.* **28**, 47 (2022).
- [46] A. Papageorgiou, G. A. Souliotis, K. Tshoo, S. C. Jeong, B. H. Kang, Y. K. Kwon, M. Veselsky, S. J. Yennello, and A. Bonasera, Neutron-rich rare isotope production with stable and radioactive beams in the mass range $A \sim 40$ –60 at beam energy around 15 MeV/nucleon, *J. Phys. G* **45**, 095105 (2018).
- [47] K. Palli, G. A. Souliotis, I. Dimitropoulos, T. Depastas, O. Fasoula, S. Koulouris, M. Veselsky, S. J. Yennello, and A. Bonasera, Microscopic description of multinucleon transfer in $^{40}\text{Ar} + ^{64}\text{Ni}$ collisions at 15 MeV/nucleon, *EPJ Web Conf.* **252**, 07002 (2021).
- [48] R. E. Tribble, R. H. Burch, and C. A. Gagliardi MARS: A momentum achromat recoil spectrometer, *Nucl. Instrum. Methods A* **285**, 441 (1989).
- [49] B. Borderie, M. F. Rivet, and L. Tassan-Got, Heavy-ion peripheral collisions in the Fermi energy domain: Fragmentation processes or dissipative collisions?, *Ann. Phys. Fr.* **15**, 287 (1990).
- [50] G. A. Souliotis, P. N. Fountas, M. Veselsky, S. Galanopoulos, Z. Kohley, A. McIntosh, S. J. Yennello, and A. Bonasera, Isoscaling of heavy projectile residues and N/Z equilibration in peripheral heavy-ion collisions below the Fermi energy, *Phys. Rev. C* **90**, 064612 (2014).
- [51] G. A. Souliotis, S. Koulouris, F. Cappuzzello, D. Carbone, A. Pakou, C. Agodi *et al.*, Identification of medium mass ($A = 60$ –80) ejectiles from 15 MeV/nucleon peripheral heavy-ion collisions with the MAGNEX large-acceptance spectrometer, *Nucl. Instrum. Methods A* **1031**, 166588 (2022).
- [52] H. Sohlbach, H. Freiesleben, W. F. W. Schneider, D. Schull, B. Kohlmeyer, M. Marinescu *et al.*, Inelastic excitation and nucleon transfer in quasielastic reactions between ^{86}Kr and ^{208}Pb at 18.2 MeV/u beam energy, *Z. Phys. A* **328**, 205 (1987).
- [53] H. Sohlbach, H. Freiesleben, W. F. W. Schneider, D. Schull, P. Braun-Munzinger, B. Kohlmeyer *et al.*, Excitation energy sharing in ^{86}Kr -induced quasielastic reactions on ^{197}Au and ^{208}Pb between 10 and 18.2 MeV/u, *Nucl. Phys. A* **467**, 349 (1987).
- [54] H. Sohlbach, H. Freiesleben, P. Braun-Munzinger, W. F. W. Schneider, D. Schull, B. Kohlmeyer *et al.*, Channel-dependent sharing of the excitation energy in quasielastic reactions between $^{208}\text{Pb} + ^{86}\text{Kr}$, *Phys. Lett. B* **153**, 386 (1985).
- [55] A. Cunsolo, F. Cappuzzello, A. Foti, A. Lazzaro, A. L. Melita, C. Nociforo *et al.*, Technique for 1st order design of a large-acceptance magnetic spectrometer, *Nucl. Instrum. Methods A* **481**, 48 (2002).
- [56] A. Cunsolo, F. Cappuzzello, A. Foti, A. Lazzaro, A. L. Melita, C. Nociforo *et al.*, Ion optics for large-acceptance magnetic spectrometers: application to the MAGNEX spectrometer, *Nucl. Instrum. Methods A* **484**, 56 (2002).
- [57] F. Cappuzzello, M. Cavallaro, A. Cunsolo, A. Foti, D. Carbone, S. E. A. Orrigo *et al.*, A particle identification technique for large acceptance spectrometers, *Nucl. Instrum. Methods A* **621**, 419 (2010).
- [58] M. Cavallaro, F. Cappuzzello, D. Carbone, A. Cunsolo, A. Foti, R. Linares *et al.*, Transport efficiency in large acceptance spectrometers, *Nucl. Instrum. Methods A* **637**, 77 (2011).
- [59] F. Cappuzzello, D. Carbone, and M. Cavallaro, Measuring the ions momentum vector with a large acceptance magnetic spectrometer, *Nucl. Instrum. Methods A* **638**, 74 (2011).
- [60] M. Cavallaro, F. Cappuzzello, D. Carbone, A. Cunsolo, A. Foti, A. Khouaja *et al.*, The low-pressure focal plane detector of the MAGNEX spectrometer, *Eur. Phys. J. A* **48**, 59 (2012).
- [61] D. Torresi, O. Sgouros, V. Soukeras, M. Cavallaro, F. Cappuzzello, D. Carbone *et al.*, An upgraded focal plane detector for the MAGNEX spectrometer, *Nucl. Instrum. Methods A* **989**, 164918 (2021).
- [62] C. Agodi, A. D. Russo, L. Calabretta, G. D'Agostino, F. Cappuzzello, M. Cavallaro *et al.*, The NUMEN project: Toward new experiments with high-intensity beams, *Universe* **7**, 72 (2021).
- [63] S. Koulouris, G. A. Souliotis, F. Cappuzzello, D. Carbone, A. Pakou, C. Agodi *et al.*, Study of the reaction ^{70}Zn (15 MeV/nucleon) + ^{64}Ni with the MAGNEX spectrometer for the production of neutron-rich isotopes, *EPJ Web Conf.* **252**, 07005 (2021).
- [64] S. Koulouris, G. A. Souliotis, F. Cappuzzello, D. Carbone, A. Pakou, C. Agodi *et al.*, Measurements of projectile fragments from $^{70}\text{Zn} + ^{64}\text{Ni}$ collisions with the MAGNEX spectrometer at INFN-LNS, *HNPS Adv. Nucl. Phys.* **28**, 42 (2022).
- [65] M. Cavallaro, C. Agodi, G. A. Brischetto, S. Calabrese, F. Cappuzzello, D. Carbone *et al.*, The MAGNEX magnetic spectrometer for double charge exchange reactions, *Nucl. Instrum. Methods B* **463**, 334 (2020).
- [66] A. Leon, S. Melki, D. Lisfi, J. P. Grandin, P. Jardin, M. G. Suraud *et al.*, Charge state distributions of swift heavy ions behind various solid targets ($36 \leq Z_p \leq 92$, $18 \text{ MeV/u} \leq E \leq 44 \text{ MeV/u}$), *At. Data Nucl. Data Tables* **69**, 217 (1998).
- [67] G. A. Souliotis, K. Hanold, W. Loveland, I. Lhenry, D. J. Morrissey, A. C. Veeck, and G. J. Wozniak, Heavy residue formation in 20 MeV/nucleon $^{197}\text{Au} - ^{12}\text{C}$ and $^{197}\text{Au} - ^{27}\text{Al}$ collisions, *Phys. Rev. C* **57**, 3129 (1998).
- [68] L. Tassan-Got and C. Stephan, Deep inelastic transfers: a way to dissipate energy and angular momentum for reactions in the Fermi energy domain, *Nucl. Phys. A* **524**, 121 (1991).

- [69] M. Papa, T. Maruyama, A. Bonasera, Constraint molecular dynamics approach to fermionic systems, *Phys. Rev. C* **64**, 024612 (2001).
- [70] M. Papa, G. Giuliani, and A. Bonasera, Constrained molecular dynamics II: An N -body approach to nuclear systems, *J. Comput. Phys.* **208**, 403 (2005).
- [71] J. Aichelin, Quantum molecular dynamics's a dynamical microscopic n -body approach to investigate fragment formation and the nuclear equation of state in heavy ion collisions, *Phys. Rep.* **202**, 233 (1991).
- [72] R. J. Charity, M. A. McMahan, G. J. Wozniak, R. J. McDonald, L. G. Moretto, D. G. Sarantites *et al.*, Systematics of complex fragment emission in niobium-induced reactions, *Nucl. Phys. A* **483**, 371 (1988).
- [73] R. J. Charity, N - Z distributions of secondary fragments and the evaporation attractor line, *Phys. Rev. C* **58**, 1073 (1998).
- [74] V. V. Volkov, Deep inelastic transfer reactions—The new type of reactions between complex nuclei, *Phys. Rep.* **44**, 93 (1978).
- [75] V. Zagrebaev and W. Greiner, Unified consideration of deep inelastic, quasi-fission and fusion-fission phenomena, *J. Phys. G: Nucl. Part. Phys.* **31**, 825 (2005).
- [76] V. Zagrebaev and W. Greiner, Low-energy collisions of heavy nuclei: dynamics of sticking, mass transfer and fusion, *J. Phys. G: Nucl. Part. Phys.* **34**, 1 (2007).
- [77] W. W. Wilcke, J. R. Birkelund, H. J. Wollersheim, A. D. Hoover, J. R. Huizenga, W. U. Schroder *et al.*, Reaction Parameters for heavy-ion collisions, *At. Data Nucl. Data Tables* **25**, 389 (1980).
- [78] G. A. Souliotis, D. J. Morrissey, N. A. Orr, B. M. Sherrill, and J. A. Winger, 0° measurements of momentum distributions of projectile-like fragments, *Phys. Rev. C* **46**, 1383 (1992).
- [79] R. Pfaff, D. J. Morrissey, M. Fauerbach, M. Hellstrom, J. H. Kelley, R. A. Kryger *et al.*, Projectilelike fragment momentum distributions from $^{86}\text{Kr} + \text{Al}$ at 70 MeV/nucleon, *Phys. Rev. C* **51**, 1348 (1995).
- [80] J. A. Scarpaci, Multiphonon states built with giant resonances, *Nucl. Phys. A* **731**, 175 (2004).
- [81] T. Depastas, G. A. Souliotis, K. Palli, A. Bonasera, and H. Zheng, A Constrained Molecular Dynamics (CoMD) study of nuclear near-ground-state properties, *EPJ Web Conf.* **252**, 07003 (2021).
- [82] M. Papa, A. Bonanno, F. Amorini, A. Bonasera, G. Cardella, A. Di Pietro *et al.*, Coherent and incoherent giant dipole resonance γ -ray emission induced by heavy ion collisions: Study of the $^{40}\text{Ca} + ^{48}\text{Ca}$ system by means of the constrained molecular dynamics model, *Phys. Rev. C* **68**, 034606 (2003).
- [83] C. Parascandolo, D. Pierroutsakou, R. Alba, A. Del Zoppo, C. Maiolino, D. Santonocito *et al.*, Evidence of dynamical dipole excitation in the fusion-evaporation of the $^{40}\text{Ca} + ^{152}\text{Sm}$ heavy system, *Phys. Rev. C* **93**, 044619 (2016).
- [84] S. Burrello, M. Colonna, and H. Zheng, The symmetry energy of the nuclear EoS: A study of collective motion and low-energy reaction dynamics in semiclassical approaches, *Front. Phys.* **7**, 53 (2019).
- [85] P. Finocchiaro, L. Acosta, C. Agodi, C. Altana, P. Amador-Valenzuela, I. Bostozun *et al.*, The NUMEN heavy ion multidetector for a complementary approach to the neutrinoless double beta decay, *Universe* **6**, 129 (2020).
- [86] F. Cappuzzello, L. Acosta, C. Agodi, I. Bostozun, G. A. Brischetto, S. Calabrese *et al.*, The NUMEN project: An update of the facility toward the future experimental campaigns, *Front. Astron. Space Sci.* **8**, 668587 (2021).
- [87] D. Calvo, I. Ciraldo, C. Agodi, F. Cappuzzello, M. Cavallaro, D. Carbone *et al.*, Present outcome from the NUMEN R&D phase, *Nucl. Instrum. Methods A* **1041**, 167336 (2022).
- [88] H. Lenske, F. Cappuzzello, M. Cavallaro, and M. Colonna, Heavy ion charge exchange reactions as probes for nuclear β -decay, *Prog. Part. Nucl. Phys.* **109**, 103716 (2019).
- [89] M. T. Magda, A. Pop, and A. Sandulescu, A model for large cluster transfer in reactions leading to heavy actinides, *J. Phys. G: Nucl. Phys.* **13**, L127 (1987).
- [90] C. Agodi, G. Giuliani, F. Cappuzzello, A. Bonasera, D. Carbone, M. Cavallaro, A. Foti, R. Linares, and G. Santagati, Analysis of pairing correlations in neutron transfer reactions and comparison to the constrained molecular dynamics model, *Phys. Rev. C* **97**, 034616 (2018).
- [91] A. Bonaccorso, Direct reaction theories for exotic nuclei: An introduction via semi-classical methods, *Prog. Part. Nucl. Phys.* **101**, 1 (2018).
- [92] I. J. Thompson, Coupled reaction channels calculations in nuclear physics, *Comput. Phys. Rep.* **7**, 167 (1988).
- [93] M. H. MacFarlane and S. C. Pieper, Ptolemy: a program for heavy-ion direct-reaction calculations, Argonne National Laboratory Report No. ANL-76-11, 1978 (unpublished).
- [94] A. Winther, Grazing reactions in collisions between heavy nuclei, *Nucl. Phys. A* **572**, 191 (1994).
- [95] A. Winther, Dissipation, polarization and fluctuation in grazing heavy-ion collisions and the boundary to the chaotic regime, *Nucl. Phys. A* **594**, 203 (1995).